Acta Crystallographica Section F
Structural Biology and Crystallization Communications
ISSN 1744-3091

Structure of human MIP-3α chemokine

Zulfiqar A. Malik[a]* and Brian F. Tack[b]

[a]Department of Pharmacology, Carver College of Medicine, The University of Iowa, Iowa City, IA 52242, USA, and [b]Department of Microbiology and Pediatrics, The University of Iowa, Iowa City, IA 52242, USA

Correspondence e-mail: z-malik@uiowa.edu

Received 2 November 2005
Accepted 24 February 2006

PDB Reference: human MIP-3α chemokine, 2hci, r2hcisf.

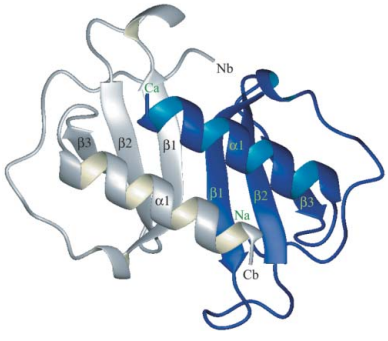

The structure of the human macrophage inflammatory protein-3α (MIP-3α) has been determined at 1.81 Å resolution by X-ray crystallography. The dimer crystallized in the tetragonal space group $I4$, with unit-cell parameters $a = b = 83.99$, $c = 57.20$ Å. The crystals exhibit two molecules in the asymmetric unit. The structure was solved by the molecular-replacement method and the model was refined to a conventional R value of 20.6% ($R_{\rm free}$ = 25.7%). MIP-3α possesses the same monomeric structure as previously described for other chemokines. However, in addition to limited structural changes in the $\beta1$–$\beta2$ hairpin of monomer B, the electron density is fully defined for a few extra residues at the N- and C-termini of monomer A and the C-terminus of monomer B compared with MIP-3α in space group $P6_1$. As the N-terminal and loop regions have been shown to be critical for receptor binding and signaling, this additional structural information may help in determining the basis of the CCR6 selectivity of MIP-3α.

1. Introduction

Leukocyte trafficking is mediated by a group of structurally related proteins known as chemokines (Rodig *et al.*, 2002). The chemokines are a group of small (8–14 kDa) basic soluble proteins that are produced and released by a wide variety of cell types during the initial phase of host response to injury, allergens, antigens or invading microorganisms (Zlotnik & Yoshie, 2000). To date, 50 chemokines and 20 receptors have been identified in humans (Zlotnik & Yoshie, 2000; Horuk, 2001). Chemokines have been identified as chemotactic cytokines and can be divided into C, CC, CXC and CX3C subgroups based upon the position of cysteine residues located near the N-terminus. Although the primary function of chemokines is the regulation of leukocyte trafficking, chemokines also play an important role in angiogenesis, tumor metastasis, hematopoiesis and human immunodeficiency virus infection (Zlotnik & Yoshie, 2000; Rollins, 1997; Baggiolini, 1998; Rossi & Zlotnik, 2000; Müller *et al.*, 2001). The chemokine macrophage inflammatory protein-3α (MIP-3α) has been noted as being expressed in human liver, lung, appendix, tonsillar crypts and skin epidermal cells (Hieshima *et al.*, 1997; Hromas *et al.*, 1997; Tanaka *et al.*, 1999; Charbonnier *et al.*, 1999). A member of the CC chemokines, MIP-3α is chemotactic for memory T cells and immature dendritic cells (Hieshima *et al.*, 1997; Varona *et al.*, 1998; Liao *et al.*, 1999; Dieu-Nosjean *et al.*, 2000; Krzysiek *et al.*, 2000), while MIP-3β is chemotactic for activated T lymphocytes and mature dendritic cells (Dieu-Nosjean *et al.*, 1999). MIP-3α and MIP-3β bind and activate CCR6 and CCR7 receptors, respectively (Yang *et al.*, 1999).

In order to identify the motifs that are key to the specificity of receptor binding and activation, various structural studies of chemokines have been made (Baldwin *et al.*, 1991; Schraufstätter *et al.*, 1993; Perez-Canadilla *et al.*, 2001; Hoover *et al.*, 2002; Luz *et al.*, 2005) by X-ray crystallography and/or NMR techniques. In this report, we present the structure of MIP-3α in the tetragonal space group $I4$ (MIPI4) at 1.81 Å resolution. Structural analysis of MIPI4 reveals subtle structural differences between the published crystal structure of human MIP-3α in space group $P6_1$ (MIPP61) at resolution 1.7 Å (Hoover *et al.*, 2002) and the current structure in space group $I4$.

Table 1
Data-measurement and refinement statistics for the structure of MIP-3α (1.81 Å).

Values in parentheses are for the outermost resolution shell (1.99–1.81 Å).

Data collection	
Crystal system	Tetragonal
Unit-cell parameters (Å)	$a = b = 83.99$, $c = 57.20$
Space group	$I4$
Resolution (Å)	21.57–1.81 (1.99–1.81)
Measured reflections	62834
Unique reflections	17465
Completeness (%)	100 (100)
$I/\sigma(I)$	15.0 (2.4)
R_{sym}† (%)	6.2 (30.8)
Solvent content (%)	61.55
No. of molecules per ASU	2
Refinement	
Resolution range (Å)	21.57–1.81
R factor (%)	20.6
R_{free} (%)	25.7
R.m.s. deviation in bond distances (Å)	0.019
R.m.s. deviation in bond angles (°)	1.7
Water molecules	128

† $R_{sym} = \sum_h \sum_i |I_{hi} - \bar{I}_h| / \sum_h \sum_i \bar{I}_h$, where I_{hi} is the observed intensity of the ith measurement of reflection h and $\bar{I}_h$ is the mean intensity of reflection h.

2. Experimental procedures

2.1. Crystallization

The chemokine macrophage inflammatory protein-3α (MIPI4) was expressed, purified and refolded as described in a previously published protocol (Schibli *et al.*, 2002).

Crystals of MIPI4 were grown by the hanging-drop vapor-diffusion method by mixing equal volumes (2 µl each) of protein (10 mg ml^{-1} in 0.1 *M* Tris–HCl pH 8.0) and reservoir solution. Two diffraction-quality crystal forms, tetragonal and hexagonal, grew together in solution No. 23 of Crystal Screen 2 (Cudney *et al.*, 1994) containing 1.6 *M* ammonium sulfate, 10%(*v*/*v*) dioxane and 0.1 *M* MES pH 6.5. Small crystals appeared within 24 h, continued to grow slowly for 10–15 d at 277 K and reached maximum dimensions in 18 d. These crystals were flash-frozen with a cryoprotectant solution [10% PEG 400, 1.6 *M* ammonium sulfate, 10%(*v*/*v*) dioxane and 0.1 *M* MES pH 6.5] for low-temperature data collection. The two crystal forms (tetragonal and hexagonal) differ only in their packing. Here, we present and discuss the structure of the tetragonal form of the crystal.

2.2. Data collection

Initial testing of the crystals for X-ray diffraction was performed on a rotating-anode RU-H3R X-ray generator equipped with state-of-the-art focusing mirrors (from Osmic) and a Rigaku R-AXIS IV^{++} image-plate detector. The diffraction data were collected (from flash-cooled crystals at 100 K) at the SBC-CAT beamline 17-ID at the Advanced Photon Source, Argonne National Laboratory. A complete data set from the tetragonal crystal form was collected by exposing a crystal to the X-ray beam for 1 s for each 0.5° oscillation. A total of 180 images were collected at 150 mm crystal-to-detector distance.

Data were processed using the program *d*TREK* (Pflugrath, 1999). The tetragonal form of the crystal belongs to space group *I*4 and diffracted to 1.81 Å. The data-collection statistics are shown in Table 1. The scaled data were truncated to obtain structure-factor amplitudes using the *CCP*4 (Collaborative Computational Project, Number 4, 1994) program *TRUNCATE* (French & Wilson, 1978).

2.3. Structure determination and refinement

The structure was solved by molecular replacement using *AMoRe* from the *CCP*4 program suite (Navaza, 1994) using the human MIP-3α dimer as a search model (PDB code 1m8a; Hoover *et al.*, 2002). A solution with a correlation coefficient of 75% and an *R* factor of 40% was obtained. Based on the calculated molecular volume (Matthews, 1968), the solvent content suggested there to be a dimer in the asymmetric unit. After an initial run of rigid-body refinement, the structure was refined using the maximum-likelihood program *REFMAC* (Murshudov *et al.*, 1997) in combination with *ARP* (Lamzin & Wilson, 1993). After a single round of refinement, the *R* factor fell to 29% with a free *R* factor of 32% (Brünger, 1992). Model building was performed using the program *O* (Jones *et al.*, 1991). All residues were shown to lie within the allowed regions of the Ramachandran plot. The final refinement statistics are given in Table 1. Validation of the structure was performed using the program *WHATIF* (Vriend, 1990) using the validation server at EMBL, Heidelberg, Germany.

3. Results and discussion

The structure of human MIP-3α has been determined by X-ray crystallography in space group *I*4. The final model of MIP-3α at 1.81 Å resolution consists of 66 residues in monomer *A* and 63 in monomer *B*, representing a total of 129 protein residues. No electron density can be seen for the first residue (Ala1) or for the side chains of the last two residues (Lys68, Asn69) of monomer *A*. In monomer *B*, the first four (Ala1–Phe4) residues and the side chains of the last two residues (Lys68, Asn69) also showed no electron density. The final crystallographic *R* factor and free *R* factor were 20.6 and 25.7%, respectively, for all reflections (21.57–1.8 Å). The r.m.s. deviations in bond lengths and bond angles are 0.019 and 1.7 Å, respectively. The Ramachandran plot calculated for the final MIP-3α model with the program *PROCHECK* (Laskowski *et al.*, 1993) shows that 95.0% of

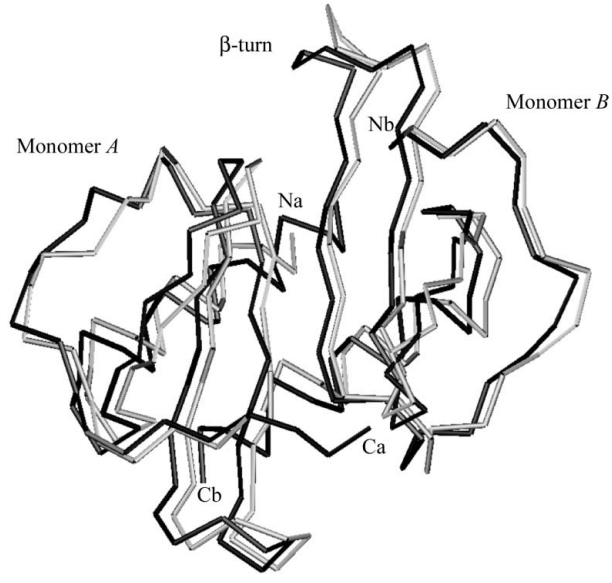

Figure 1
Superimposed C$^{\alpha}$ backbone structures of human MIPP61 in grey and MIPPI4 in black showing the long N- and C-termini of monomer *A*. The alternative orientation of the β-turn can also be seen in monomer *B*. The r.m.s. difference in Asp5–Lys65 C$^{\alpha}$ atomic positions, calculated with the *LSQMAN* option in *O*, is 0.85 Å (Jones *et al.*, 1991). This figure was created using the program *MOLMOL* (Koradi *et al.*, 1996).

the residues are in the most favored regions and 5.0% of residues are in the additionally allowed regions.

3.1. Description of the tertiary structure of the monomer

MIPI4 possesses the same monomeric structure previously described for other chemokines. The N-terminal region is attached to the β_1–β_2 loop (Leu27–Asn35) and the β_3 strand (Ser46–Ala49) by the disulfide bonds 6–32 and 7–48. Other interactions between the N-terminus and the core of the protein include the main-chain N and O atoms of Cys7 with Gln26 of the β_1 strand. The main-chain N atom of Thr11 also forms a hydrogen bond with the main-chain O atom of Cys48 of the β_3 strand.

Superposition of MIPI4 on to the structure of MIPP61 shows limited but significant structural differences at the N-terminus of monomer *A* and in the β-turn loop between the β_1 and β_2 strands of monomer *B* (Fig. 1). The primary differences between MIPP61 and MIPPI4 lie in the electron density for previously undefined residues at the N-terminus of monomer *A* and the C-terminal helices in both monomers *A* and *B* of MIPI4. The conformation of the Asn27–Cys33 loop between the β_1 and β_2 strands is slightly different in monomer *B* of MIPI4, where Arg25 and Glu30 brace each other by forming a hydrogen bond between the side-chain OE1 and OE2 atoms of Glu30 and the NH1 and NH2 of Arg25 of the same monomer *B*. This interaction may play some role in the bend of the β-turn towards the core of the protein. Glu30 OE1 forms another hydrogen bond with water in the same monomer *B*, while Glu30 OE2 may stabilize the dimer by forming a hydrogen bond with the side chain of Lys42 in an adjacent monomer *A*. In MIPP61 the side chain of Glu30 of monomer *B* is exposed to water, while Arg25 is oriented inward, forming a hydrogen bond with a water molecule and main-chain O atom of Leu63 of the C-terminal α-helix in monomer *A*. The hydrophobic interaction of the side chains of the C-terminal helix with the β-sheet is similar to those in MIPP61 except that Leu15 is facing Phe19 and Ile20. These differences may arise as a consequence of the different packing of the molecules in the crystal.

3.2. Description of dimerization in the crystal

The dimerization in the MIP-3α crystal structure is similar to that seen in several CXC chemokines (Baldwin *et al.*, 1991). The dimer is primarily stabilized by hydrogen bonds between the β_1 strands of the two monomers as well as by additional side-chain interactions. Thus, the dimeric molecule consists of a six-stranded sheet and two anti-parallel helices inclined at an angle of $\sim$60° to the β-strands (Fig. 2). Several hydrogen-bond interactions between monomers *A* and *B* are similar to those seen in MIPP61.

Several studies have shown interaction between the amino-terminus of chemokines (MIP-1α and RANTES) and the trans-membrane helix bundle of the cellular receptors, such as CCR5 (Murphy *et al.*, 2000; Rollins, 1997; Zlotnik & Yoshie, 2000; Blanpain *et al.*, 2003). Amino-acid residues preceding the first cysteine and the N-loop (second receptor-binding site, residues 10–20) of chemokines are important for binding and receptor activation (Clark-Lewis *et al.*, 1995; Lowman *et al.*, 1996). We found fully defined electron density for the N-terminal Ser2, Asn3 and Phe4 of monomer *A* that was not visible in MIPP61. These well defined residues of monomer *A* may play a role in stabilization of the dimer, as the side-chain O atom of Ser2 and the main-chain O atom of Asn3 of monomer *A* form two hydrogen bonds with the side chain of Lys44 of monomer *B* (Fig. 3). Residues 41–44 of the loop between strands β_2 and β_3 of monomer *B* are also shifted, perhaps as a consequnce of the presence of Phe4 in monomer *A*. This probably results in restricting the freedom of this loop in monomer *B*. The dimer in MIPI4 is further stabilized by the weak hydrogen bond between the side chain of Glu30 of monomer *A* and Lys42 of monomer *B* (Fig. 3).

Studies on IL-8, which is structurally related to MIP-3α, suggest that the C-terminus also plays an important role in binding to receptors (Schraufstätter *et al.*, 1993), indicating that the C-terminus could be important for the function of the chemokine. The orientation of the C-terminal helix to the triple-stranded β-sheet within each monomer is stabilized by a number of hydrophobic interactions. There are hydrophobic contacts between Val67 of the C-terminus of monomer *A* and the methyl groups of Val60 and Ile37 from the β2 strand of monomer *B*. There is also a hydrogen bond between Arg61 of monomer *A* and Ser64 of monomer *B*, while Arg61 of monomer *B*

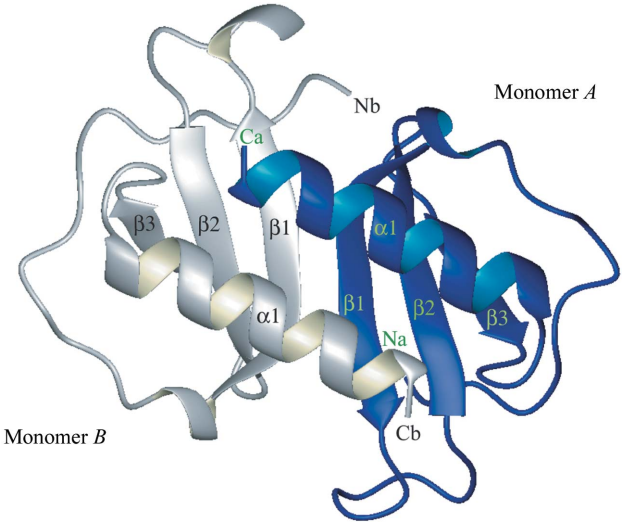

Figure 2
Ribbon diagram of the overall three-dimensional structure of the dimer of human MIP-3α. The dimer is composed of a six-stranded β-sheet and two parallel α-helices. β-Strands are shown as arrows and α-helices as coils. This figure was generated with the program *MOLMOL* (Koradi *et al.*, 1996).

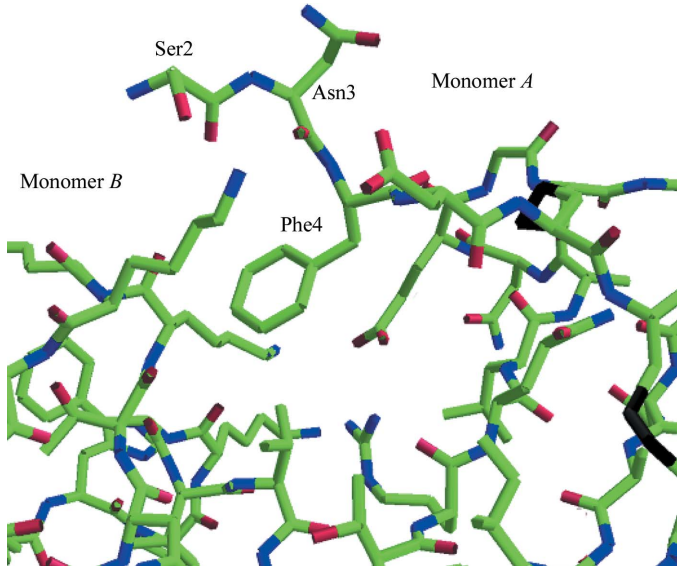

Figure 3
Stick representation of the well defined N-terminal residues Ser2, Asn3 and Phe4 of monomer *A* that may play a role in the stabilization of the dimer.

makes a van der Waals interaction with Ser64 of monomer *A*. These interactions may serve to maintain the orientation of the C-terminal helices with respect both to each other and to the β-sheet below. In MIPI4 the long C-terminal helix forms two more hydrogen bonds between the side-chain N atom of Lys57 of monomer *A* and the main-chain O atom of Val67 of monomer *B*. Likewise, the main-chain O atom of Val67 of monomer *A* forms a hydrogen bond with the side chain of Lys57 of monomer *B*. These side-chain interactions are different from those seen in MIPP61 (Hoover *et al.*, 2002).

Structural analysis of chemokines has revealed that the α/β-fold is highly conserved between both the CXC and CC chemokine classes (Schraufstätter *et al.*, 1993). The electron-density map was ambiguous for N- and C-terminus residues in MIPP61, but is significantly clearer in the MIPI4 structure, especially at the amino-terminus, which comprises one of the receptor-recognition and binding motifs. We have also identified two residues at the C-terminus of both monomers that were disordered and could not be interpreted in MIPP61.

These new experimentally observed side-chain interactions, especially the significant differences at the N-terminus and β-turn of monomer *B*, coupled with the C-terminal hydrophobic interactions may help to increase our understanding of the interaction between chemokines and their receptors. These results will also aid the rational design of variants to modulate or interfere with its important biological functions.

We thank the protein crystallography facility and Dr S. Ramaswamy at the Department of Biochemistry, University of Iowa for help during data collection. Use of the Advanced Photon Source was supported by the US Department of Energy, Office of Science, Office of Basic Energy Sciences under Contract No. W-31-109-Eng-38.

References

Baggiolini, M. (1998). *Nature (London)*, **392**, 565–568.

Baldwin, E. T., Weber, I. T., St Charles, R., Xuan, J. C., Appella, E., Yamada, M., Matsushima, K., Edwards, B. F., Clore, G. M. & Gronenborn, A. M. (1991). *Proc. Natl Acad. Sci. USA*, **88**, 502–506.

Blanpain, C., Doranz, J. B., Bondue, A., Govaerts, C., De Leener, A., Vassart, G., Doms, W. R., Proudfoot, A. & Parmentier, M. (2003). *J. Mol. Biol.* **278**, 5179–5187.

Brünger, A. T. (1992). *Nature (London)*, **355**, 472–474.

Charbonnier, A. S., Kohrgruber, N., Kriehuber, E., Stingl, G., Rot, A. & Maurer, D. (1999). *J. Exp. Med.* **190**, 1755–1767.

Clark-Lewis, I., Kim, K. S., Rajarathnam, K., Gong, J. H., Dewald, B., Moser, B., Baggiolini, M. & Sykes, B. D. (1995). *J. Leukoc. Biol.* **57**, 703–711.

Collaborative Computational Project, Number 4 (1994). *Acta Cryst.* D**50**, 760–763.

Cudney, R., Patel, S., Weisgraber, K., Newhouse, Y. & McPherson, A. (1994). *Acta Cryst.* D**50**, 414–423.

Dieu-Nosjean, M. C., Massacrier, C., Homey, B., Vanbervliet, B., Pin, J. J., Vicari, A., Lebecque, S., Dezutter-Dambuyant, C., Schmitt, D., Zlotnik, A. & Caux, C. (2000). *J. Exp. Med.* **192**, 705–717.

Dieu-Nosjean, M. C., Vicari, A., Lebecque, S. & Caux, C. (1999). *J. Leukoc. Biol.* **66**, 252–262.

French, G. S. & Wilson, K. S. (1978). *Acta Cryst.* A**34**, 517–525.

Hieshima, K., Imai, T., Opdenakker, G., Van Damme, J., Kusuda, J., Tei, H., Takasuki, K., Miura, R., Yoshie, O. & Nomiyama, H. (1997). *J. Biol. Chem.* **272**, 5846–5853.

Hoover, D. M., Boulègue, C., Yang, D., Oppenheim, J. J., Tucker, K., Lu, W. & Lubkowski, J. (2002). *J. Biol. Chem.* **277**, 37647–37654.

Horuk, R. (2001). *Cytokines Growth Factors Rev.* **12**, 313–335.

Hromas, R., Gray, P. W., Chantry, D., Godiska, R., Krathwohl, M., Fife, K., Bell, I., Takeda, J., Aronica, S., Gordon, M., Cooper, S., Broxmeyer, H. E. & Klemsz, M. J. (1997). *Blood*, **89**, 3315–3322.

Jones, T. A., Zou, J. Y., Cowan, S. W. & Kjeldgaard, M. (1991). *Acta Cryst.* A**47**, 110–119.

Koradi, R., Billeter, M. & Wüthrich, K. (1996). *J. Mol. Graph.* **14**, 51–55.

Krzysiek, R., Lefevre, E. A., Bernard, J., Foussat, A., Galanaud, P., Louache, F. & Richard, Y. (2000). *Blood*, **96**, 2338–2345.

Lamzin, V. & Wilson, K. S. (1993). *Acta Cryst.* D**49**, 129–147.

Laskowski, R. A., MacArthur, M. W., Moss, D. S. & Thornton, J. M. (1993). *J. Appl. Cryst.* **26**, 283–290.

Liao, F., Rabin, R. L., Smith, C. S., Sharma, G., Nutman, T. B. & Farber, J. M. (1999). *J. Immunol.* **162**, 186–194.

Lowman, H. B., Stagele, P. H., Deforgo, L. E., Wirth, C. M., Gillece-Castro, B. L., Bourell, J. H. & Fairbrother, W. J. (1996). *J. Biol. Chem.* **271**, 14344–14352.

Luz, J. G., Yu, M., Su, Y., Wu, Z., Zhou, Z., Sun, R. & Wilson, I. A. (2005). *J. Mol. Biol.* **352**, 1019–1028.

Matthews, B. W. (1968). *J. Mol. Biol.* **33**, 491–497.

Müller, A., Homey, B., Soto, H., Ge, N., Catron, D., Buchanan, M. E., McClanahan, T., Murphy, E., Yuan, W., Wagner, S. N., Barrera, J. L., Mohar, A., Verástegui, E. & Zlotnik, A. (2001). *Nature (London)*, **410**, 50–56.

Murphy, P. M., Baggiolini, M., Charo, I. F., Hebert, C. A., Horuk, R., Matsushima, K., Miller, L. H., Oppenheim, J. J. & Power, C. A. (2000). *Pharmacol. Rev.* **52**, 145–176.

Murshudov, G. N., Vagin, A. A. & Dodson, E. J. (1997). *Acta Cryst.* D**53**, 240–255.

Navaza, J. (1994). *Acta Cryst.* A**50**, 157–163.

Perez-Canadilla, J. M., Zaballaos, A., Gutierrez, J., Varona, R., Roncal, F., Albar, J. P., Marquez, G. & Bruix, M. (2001). *J. Biol. Chem.* **276**, 28372–28379.

Pflugrath, J. W. (1999). *Acta Cryst.* D**55**, 1718–1725.

Rodig, S. J., Jones, D., Shahsafaei, A. & Dorfman, D. M. (2002). *Hum. Pathol.* **33**, 1227–1233.

Rollins, B. J. (1997). *Blood*, **90**, 909–928.

Rossi, D. & Zlotnik, A. (2000). *Annu. Rev. Immunol.* **18**, 217–242.

Schibli, J. D., Hunter, H. N., Aseyev, V., Starner, T. D., Wiencek, J. M., McCray, P. B. Jr, Tack, B. F. & Vogel, H. J. (2002). *J. Mol. Biol.* **277**, 8279–8289.

Schraufstätter, I. U., Barritt, D. S., Ma, M., Oades, Z. G. & Cochrane, C. G. (1993). *J. Immunol.* **151**, 6418–6428.

Tanaka, Y., Imai, T., Baba, M., Ishikawa, I., Uehira, M., Nomiyama, H. & Yoshie, O. (1999). *Eur. J. Immunol.* **29**, 633–642.

Varona, R., Zaballos, A., Gutierrèz, J., Martin, P., Roncal, F., Albar, J. C., Ardavin, C. & Màrquez, G. (1998). *FEBS Lett.* **440**, 188–194.

Vriend, G. (1990). *J. Mol. Graph.* **8**, 52–56.

Yang, D., Chertov, O., Bykovskaia, S. N., Chen, Q., Buffo, M. J., Shogan, J., Anderson, M., Schöder, J. M., Wang, J. M., Howard, O. M. Z. & Oppenheim, J. J. (1999). *Science*, **286**, 525–528.

Zlotnik, A. & Yoshie, O. (2000). *Immunity*, **12**, 121–127.